Available online at www.sciencedirect.com
SCIENCE DIRECT®
Nuclear Instruments and Methods in Physics Research A 512 (2003) 52–59
NUCLEAR INSTRUMENTS & METHODS IN PHYSICS RESEARCH Section A
www.elsevier.com/locate/nima

New evidence of dominant processing effects in standard and oxygenated silicon diodes after neutron irradiation

A. Candelori[a,*], R. Rando[a], D. Bisello[a], F. Campabadal[b], V. Cindro[c], L. Fonseca[b], A. Kaminski[a], A. Litovchenko[b], M. Lozano[b], C. Martínez[b], A. Moreno[b], J.M. Rafi[b], J. Santander[b], M. Ullán[b], J. Wyss[d]

[a] *Dipartimento di Fisica, Istituto Naz. Di Fisica Nucleare (INFN), Sezione di Padova, Via Marzolo 8, I-35100 Padova, Italy*
[b] *Institut de Microelectronica de Barcelona (IMB-CNM-CSIC), Cerdanyola del Valles, E-08193 Barcelona, Spain*
[c] *Jožef Stefan Institute, Jamova 39, SI-1000 Ljubljana, Slovenia*
[d] *Dipartimento di Meccanica, Struttura, Ambiente e Territorio, via DiBiasio 43, I-03043 (FR) Cassino, Italy*

Abstract

Silicon diodes processed on standard and oxygenated silicon substrates by three different manufacturers have been irradiated by neutrons in a nuclear reactor. The leakage current density (J_D) increase is linear with the neutron fluence. J_D and its annealing curve at 80°C do not present any sizeable dependence on substrate oxygenation and/or manufacturing process. The acceptor introduction rate (β) of the effective substrate doping concentration (N_{eff}) is independent from the oxygen concentration when standard and oxygenated devices from the same manufacturer are considered. On the contrary, β significantly varies from one manufacturer to another showing that the β dependence on the particular process can be important, overtaking the small substrate oxygenation effect. Finally, the average saturation value of the N_{eff} reverse annealing is slightly lower for the oxygenated samples, pointing out a positive effect of the substrate oxygenation even for devices irradiated by neutrons.

Keywords: Semiconductor diodes; Radiation detectors; Neutron radiation damage

1. Introduction

In the High Energy Physics experiments at the CERN Large Hadron Collider (Geneve, Switzerland) the microstrip silicon detectors will be exposed to high hadron (protons, pions and neutrons) fluxes. It has been estimated [1] that in the experiment lifetime of 10 years, the CMS silicon tracker will undergo fluences equivalent to 1 MeV neutrons up to 1.6×10^{13} neutrons/(cm$^2 \cdot$ year). The damage induced by hadrons in the silicon detector bulk causes detector performance degradations due to the increase of the leakage current (J_D) [2–11] and, after space charge sign inversion (SCSI), of the depletion voltage (V_{dep}) [3–17]. Moreover in irradiated devices J_D and V_{dep} are not stable at room temperature (RT): while J_D monotonically decreases, V_{dep} starts

*Corresponding author. Tel.: +39-049-8277215; fax: +39-049-8277237.
E-mail address: candelori@pd.infn.it (A. Candelori).

0168-9002/03/$ - see front matter
doi:10.1016/S0168-9002(03)01876-X

to increase $\approx$10–20 days after irradiation as a consequence of the reverse annealing effect [3–6,12,15,17], which at RT continues for many years. The V_{dep} increase is consequently a central problem, taking into account that detectors will operate in over-depletion to maximize the charge collection, and high bias voltages can lead the detector to junction breakdown.

The RD48 (ROSE) collaboration at CERN [18,19] has widely investigated the "substrate oxygenation effects", i.e., how the V_{dep} increase can be mitigated by the introduction of high oxygen concentrations ($[O] > 10^{17}\,cm^{-3}$) in the silicon bulk before diode processing. The substrate oxygenation has a beneficial effect when devices are exposed to charged hadrons (protons and pions) [6–11,13,14,16–19], because oxygen reacts with radiation induced vacancies (V), preventing the formation of the electrically active V–V defects which contribute to the V_{dep} increase and to the reverse annealing. On the other hand, the oxygen mitigating effect is absent when devices are irradiated by neutrons because neutron induced defects are produced in clusters, where the defect density is orders of magnitude higher than the highest achievable oxygen concentration [16,17].

In previous studies [8–11] we reported on the V_{dep} increase rate for oxygenated and standard devices after irradiation by 16 MeV, 27 MeV and 24 GeV protons: substrate oxygenation always mitigates the V_{dep} increase rate to values that are almost independent from the manufacturer, while a wide range of values is present if standard devices processed by different manufacturers are considered. This suggests that not only the oxygen concentration but also processing affects the diode radiation hardness after proton irradiations.

The purpose of this contribution is to extend our previous studies by disentangling the effects of processing and substrate oxygenation: standard and oxygenated diodes from three different manufacturers have been irradiated by nuclear reactor neutrons, which are not expected to produce sizeable effects in oxygenated devices with respect to diodes processed on standard substrates, highlighting process effects in the induced bulk damage characteristics.

Table 1
Diode characteristics

Diode label	Manufacturer	Substrate oxygenation	[O] (cm^{-3})	Resistivity ($k\Omega\,cm$)
M_{STD}	Micron	No	$<4\times10^{16}$	15
M_{OXY}	Micron	1150°C, 110 h	$\approx2.5\times10^{17}$	2.4
ST_{STD}	ST	No	$<4\times10^{16}$	2
ST_{OXY}	ST	1200°C, 30 h	$2–2.5\times10^{17}$	2
CNM_{STD}	CNM	No	$<4\times10^{16}$	4
CNM_{OXY}	CNM	1150°C, 60 h	$\approx2\times10^{17}$	4

2. Devices

Tested devices are p^+–n silicon diodes processed by three different manufacturers (CNM [20], ST Microelectronics [21], and Micron Semiconductor [22]) on standard ($[O]\leqslant4\times10^{16}\,cm^{-3}$) and oxygenated ($[O]\geqslant10^{17}\,cm^{-3}$) n-type high resistivity ($\rho\geqslant2\,k\Omega\,cm$) silicon substrates. The diode thickness is 280 μm for CNM diodes and 300 μm for ST and Micron devices. Each diode is surrounded on the junction side by a p^+ guard-ring, which defines the device active area: 0.25 cm^2 for CNM and ST diodes, 0.15 cm^2 for Micron devices.

The substrate oxygenation was performed before processing by oxygen diffusion at high temperature ($>1000°C$) from sacrificial SiO_2 layers thermally grown on each wafer side [5–7,16,17,23,24]. The oxygenation process characteristics and the diode substrate resistivity are summarized in Table 1. The oxygen concentration in the substrate has been determined by Secondary Ion Mass Spectrometry (SIMS) measurements from the manufacturers.

3. Irradiation conditions

Devices were irradiated by neutrons in the Triga MARK II nuclear reactor of the Jožef Stefan Institute (Lubjana, Slovenia). The neutron fluence has been determined by previous gold activation calibration measurements [25] performed in the same experimental conditions (geometry and reactor power). The neutron energy spectrum in the nuclear reactor extends from thermal to fast ($\approx$10 MeV) neutrons and the fluences reported in

the paper refer to the fast neutron component ($E \geqslant 100$ keV) plus a 1.5% correction accounting for the non-ionizing energy loss (NIEL) of the $E < 100$ keV neutron component [25].

Devices were irradiated in single steps, i.e., different devices were considered for each neutron fluence. After irradiation devices were annealed at 80°C for 4 min in an ambient atmosphere oven in order to complete the beneficial annealing of the effective substrate doping concentration and to reach the minimum V_{dep} value after the beneficial annealing, but before the reverse annealing process activation [6,7,13].

The diodes were electrically characterized before irradiation and after the 80°C annealing by 10 kHz capacitance–voltage ($C-V$) and current–voltage ($I-V$) measurements. The $C-V$ and $I-V$ measurements were performed by an HP4284A LCR meter and by an HP4142B DC source/monitor, respectively. During the electrical characterization devices were reverse biased by applying a positive voltage to the backside contact, while the p^+ junction contact and the p^+ guard-ring were separately grounded, in order to prevent border effects on the measurements of the diode sensitive volume current and capacitance.

4. Leakage current density

The diode current density at full depletion is defined as $J_D = I/(A \cdot W)|_{V=V_{dep}}$, where I is the diode reverse leakage current, A is the diode area, W is the diode thickness and V_{dep} is the diode depletion voltage. The diode reverse leakage current strongly depends on temperature and in our study all the measurements have been scaled to 20°C according to [26–28]

$$I(T_R) = I(T)(T_R/T)^2 \times \exp[(-E/2k_B)(1/T_R - 1/T)] \quad (1)$$

where T is the absolute temperature during the $I-V$ measurement, $T_R = 293.16$ K (20°C), k_B is the Boltzmann constant, and the E parameter is 1.23 eV, as suggested in Ref. [28]. The diode depletion voltage has been determined as the intersection point of the two linear fits before and after the kink of the 10 kHz $C-V$ curve on a log–log scale [3,4,15,16].

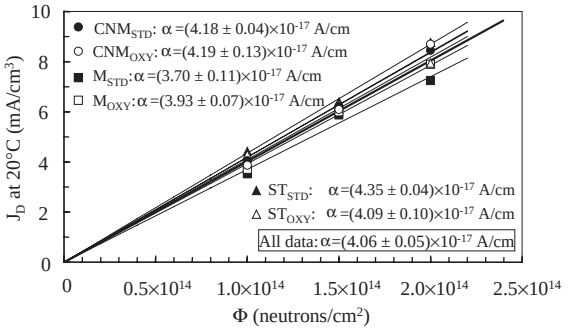

Fig. 1. Diode current density at full depletion scaled to 20°C as a function of the neutron fluence for standard (closed symbols) and oxygenated (open symbols) diodes processed by CNM (circle), Micron (squares) and ST (triangles). Each line is a linear fit, whose slope, i.e. the current density increase rate α, is also reported. The longer solid line is the linear fit of all the reported data.

The diode current density scaled to 20°C as a function of the neutron fluence is shown in Fig. 1. As expected the leakage current density linearly increases with the particle fluence [2–11]

$$J_D = J_0 + \alpha \cdot \Phi \quad (2)$$

where α is the leakage current density increase rate and J_0 (≈ 10 nA/cm^3) is the diode current density before irradiation, which is negligible in our study. The α values for the different devices are in good agreement among them (within 10%), the small dispersion being mainly due to the scattered J_D data at the highest fluence. No systematic trend is observed for standard and/or oxygenated devices from the three manufacturers, in agreement with the result that the leakage current density increase rate is independent of processing and/or substrate oxygenation [2,4,5].

The α value determined by considering the linear fit of all the data in Fig. 1 (4.06 ± 0.05 A/cm) has been considered to determine the hardness factor [26] of the nuclear reactor neutron source with respect to 1 MeV neutrons, according to the NIEL scaling hypothesis

$$\alpha(n_R)/\alpha(n_{1\,Mev}) = K(n_R)/K(n_{1\,Mev}) \quad (3)$$

where $\alpha(n_R)$ and $K(n_R)$ are the leakage current density increase rate and the radiation hardness

factor of nuclear reactor neutrons, respectively, while $\alpha(n_{1\,\mathrm{MeV}}) = 4.56 \times 10^{-17}\,\mathrm{A/cm}$ [29] and $K(n_{1\,\mathrm{MeV}}) = 1$ are the corresponding values for 1 MeV neutrons. We obtain $K(n_R) = 0.89 \pm 0.01$, in very good agreement with the expected result $K(n_R) = 0.88 \pm 0.05$ [30].

5. Effective substrate doping concentration

The diode depletion voltage is proportional to the absolute value of the effective substrate doping concentration (N_{eff}):

$$|N_{\mathrm{eff}}| = 2\varepsilon(V_{\mathrm{dep}} - V_{\mathrm{bi}})/(qW^2) \quad (4)$$

where ε is the absolute silicon dielectric constant, q is the electron charge, W is the diode thickness, $V_{\mathrm{bi}} \approx 0.6\,\mathrm{V}$ is the junction built-in potential and in our study $V_{\mathrm{dep}} > V_{\mathrm{bi}}$. Defects generated in the diode substrate by neutrons cause the variation of the effective substrate doping concentration and consequently of V_{dep}. The two microscopic mechanisms related to the N_{eff} variation are the donor removal (in n-type silicon) and the deep acceptor level generation, which are macroscopically modeled as a function of the neutron fluence (Φ) by [3,4,7,15]

$$N_{\mathrm{eff}} = N_0 e^{-c\Phi} - \beta\Phi \quad (5)$$

where N_0 is the donor concentration before irradiation, c is the donor removal coefficient and β is the acceptor introduction rate. By increasing Φ, N_{eff} decreases up to the condition $N_0 e^{-c\Phi} = \beta\Phi$, then SCSI occurs, i.e., N_{eff} becomes negative. After SCSI, $N_0 e^{-c\Phi} \ll \beta\Phi$, i.e., $|N_{\mathrm{eff}}| \propto \beta \cdot \Phi$, and the slope of the $N_{\mathrm{eff}}(\Phi)$ curve is a direct measurement of the acceptor introduction rate.

The effective substrate doping concentration as a function of the neutron fluence is shown in Fig. 2 for the different manufacturers. The β values of the standard and oxygenated Micron devices are quite compatible, as expected [5,6], pointing out that no significant difference appears for devices processed by Micron on standard and oxygenated substrates when irradiated by neutrons. Similarly, also the β values of the standard and oxygenated CNM diodes are compatible, but slightly lower than the Micron device data, pointing out the manufacturer process dependence after neutron irradiation, whereas substrate oxygenation effects do not influence β when standard and oxygenated devices from the same manufacturer are considered.

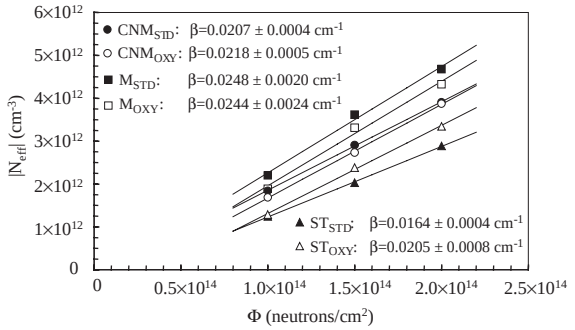

Fig. 2. Absolute value of the effective substrate doping concentration as a function of the neutron fluence for standard (closed symbols) and oxygenated (open symbols) diodes processed by CNM (circles), Micron (squares) and ST (triangles). The slope of each linear fit, i.e. the acceptor introduction rate β, is also reported. The β error refers to the fit inaccuracy.

The standard ST diodes present the lowest β value, confirming that the dependence of the acceptor introduction rate on the particular process is the most important effect for devices irradiated by neutrons. The effect of the ST_{STD} β, which is lower than the corresponding ST_{OXY} value, is more to be attributed to a variation of the ST process for the long time interval (≈ 3 years) in the different batch productions than to a negative effect, never observed, of the substrate oxygenation. This is a further evidence of the importance of process related effects on the acceptor introduction rate.

6. Test of the NIEL scaling hypothesis for β

The NIEL scaling hypothesis for β foresees that the acceptor introduction rate must be the same for any device and irradiation source when the nominal fluence is normalized to the 1 MeV neutron equivalent value. The fluence normalization is performed by dividing the nominal fluence for the radiation hardness factor or more accurately for the ratio of the measured leakage

Table 2
β and β_{Norm} values for the different diodes

Diode label	β (cm^{-1})	β_{Norm} (cm^{-1})
CNM_{STD}	0.0207 ± 0.0004	0.0226 ± 0.0005
CNM_{OXY}	0.0218 ± 0.0005	0.0237 ± 0.0009
M_{STD}	0.0248 ± 0.0020	0.0305 ± 0.0026
M_{OXY}	0.0244 ± 0.0024	0.0283 ± 0.0028
ST_{STD}	0.0164 ± 0.0004	0.0172 ± 0.0005
ST_{OXY}	0.0205 ± 0.0008	0.0229 ± 0.0010

current density increase rate to that of 1 MeV neutrons. The acceptor introduction rate after fluence normalization can be calculated by $\beta_{Norm} = \beta \cdot \alpha(n_{1\,MeV})/\alpha$ with the advantage that it accounts also for the data dispersion of the leakage current density increase rate, shown in Fig. 1 for the different diode types.

The β_{Norm} values of the devices taking into account the fits in Figs. 1 and 2 are reported in Table 2. The quoted errors come from the propagation of the corresponding α and β fit errors. The β_{Norm} values of standard and oxygenated CNM (or Micron) diodes are compatible within errors. Nevertheless, the β_{Norm} values are not compatible if data from different manufacturers are compared, pointing out the inadequacy of the NIEL scaling hypothesis for the acceptor introduction rate after neutron irradiation due to process related effects.

7. N_{eff} reverse annealing and J_D annealing

After irradiation N_{eff} and J_D depend on time and temperature. At room temperature (RT) J_D monotonically decreases due to the annealing of the defects responsible for the leakage current generation. On the contrary, N_{eff} initially decreases up to a plateau reached $\approx$10–20 days after the end of irradiation due to the beneficial annealing and then it starts to increase as a consequence of the reverse annealing effect [4]. This phenomenon is related to the mobility of the radiation induced vacancies, which are not frozen at RT: mobile vacancies can generate divacancy complexes, causing V_{dep} to increase even after the end of the irradiation.

The time evolution of J_D and N_{eff} after irradiation have been studied for diodes irradiated at the intermediate fluence (1.50×10^{14} neutrons/cm^2) by isothermal annealing of the devices at $T = 80°C$ in nine cumulative steps: 4, 8, 16,…, 1024 min. Devices were heated in an oven in ambient atmosphere and then electrically characterized at RT by $I-V$ and $C-V$ measurements after each annealing step, in order to determine the corresponding J_D and N_{eff} values. The 80°C temperature presents an acceleration factor of 7400 [19] with respect to the reverse annealing at RT, i.e. 365 days at RT correspond to $\approx$71 min at 80°C.

7.1. N_{eff} reverse annealing

The evolution of the effective substrate doping concentration as a function of the annealing time (t) at 80°C with respect to its minimum value (occurring at t_{min}), i.e. $|\Delta N_{eff}(t)| = |N_{eff}(t) - N_{eff}(t_{min})|$, is reported in Fig. 3. The V_{dep} variations between $t = 4$ and 8 min are lower than 4 V confirming that the plateau region of the depletion voltage is already reached after the first annealing step. The $|\Delta N_{eff}|$ data rapidly increase up to the 7th annealing step (256 min), then for $t > 256$ min a saturation trend can be observed.

The $|\Delta N_{eff}|$ evolution as a function of the annealing time has been determined to be a first-order process [4,12,15], which can be fitted by the function

$$|\Delta N_{eff}(t)| = N_C \cdot (1 - \exp(-[t - t_0]/\tau)) \quad (6)$$

where N_C is the maximum variation (amplitude) of the reverse annealing, τ is the process time constant and t_0 is the annealing time at which the reverse annealing starts to appear. The reverse annealing fit parameters of Eq. (6) minimizing the least squares from the data shown in Fig. 3 are reported in Table 3.

The experimental data of the CNM and ST diodes are very close together and consequently the corresponding fit parameters are compatible within errors, if standard (or oxygenated) devices from these two manufacturers are considered. This suggests that CNM and ST processes are similar for the reverse annealing process, even if the

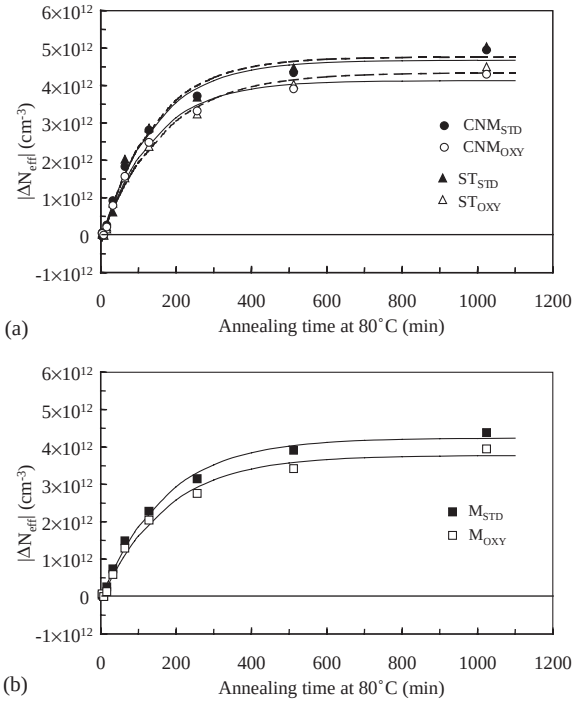

Fig. 3. Variation of the effective substrate doping concentration as a function of the annealing time at 80°C for standard (closed symbols) and oxygenated (open symbols) diodes processed by CNM (circles), Micron (squares) and ST (triangles). The solid (for CNM and Micron) and dotted (for ST) lines are the fits of the experimental data by the function $|\Delta N_{\text{eff}}| = N_C \cdot (1 - \exp(-[t - t_0]/\tau))$, whose parameters are reported in Table 3.

Table 3
Parameters of the reverse annealing fit: $N_C \cdot (1 - e^{-(t-t_0)/\tau})$ for standard and oxygenated diodes

Diode	N_C (10^{12} cm^{-3})	τ (min)	t_0 (min)
CNM_{STD}	4.68 ± 0.18	138 ± 20	5.0 ± 4.7
M_{STD}	4.24 ± 0.14	167 ± 20	3.1 ± 4.6
ST_{STD}	4.76 ± 0.13	136 ± 25	7.3 ± 5.7
CNM_{OXY}	4.13 ± 0.13	136 ± 16	5.9 ± 3.4
M_{OXY}	3.78 ± 0.15	169 ± 24	5.1 ± 5.5
ST_{OXY}	4.34 ± 0.16	162 ± 22	3.9 ± 5.0

acceptor introduction rate is lower for ST standard diodes.

The experimental data of the Micron diodes are slightly lower than the CNM and ST devices if standard (or oxygenated) samples are compared, suggesting that the Micron process is less sensitive to the formation of defects contributing to the reverse annealing process after neutron irradiation. The difference between the $|\Delta N_{\text{eff}}(t)|$ standard (oxygenated) curves of the CNM or ST diodes with respect to the Micron devices increases by increasing the annealing time, but in any case the CNM, ST and Micron standard (oxygenated) data are within 10% from the average data of the standard (oxygenated) samples.

The reverse annealing amplitude (N_C) is systematically lower for oxygenated than for standard devices produced by the same manufacturer, suggesting a small positive effect of the substrate oxygenation even after neutron irradiation: oxygen captures vacancies during the reverse annealing also for neutron irradiated devices by the formation of V–O complexes, slightly mitigating the V–V defect generation and the V_{dep} increase during the reverse annealing. On the contrary, the τ and t_0 parameters are not significantly affected by manufacturing process and/or by substrate oxygenation, being all the reported values compatible within the fit errors.

Standard ST devices, whose β value is lower than all the other diodes (see Fig. 2), present the highest reverse annealing amplitude. This result points out that even if the acceptor introduction rate is influenced by process related effects which overcome the substrate oxygenation, the reverse annealing amplitude is mainly dependent on the substrate oxygenation.

7.2. J_D annealing

The $J_D(t)$ annealing data for devices irradiated at the intermediate fluence have been reported in Fig. 4, where the $J_D(t)$ curves are normalized to the value after the first annealing step, i.e. $J_D(t)/J_D(4\,\text{min})$, in order to remove the effect of the data dispersion on $J_D(t)$ (see Fig. 1).

The leakage current density continuously decreases by increasing t due to the annealing of the radiation induced microscopic defects responsible for the generation current. The $J_D(t)/J_D(4\,\text{min})$ curves are close together pointing out that the annealing of the microscopic defects is not dependent on processing and/or oxygenation.

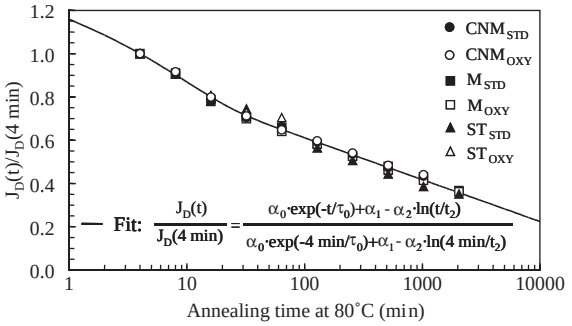

Fig. 4. $J_D(t)/J_D(4\,\text{min})$ as a function of the annealing time at 80°C for standard (closed symbols) and oxygenated (open symbols) diodes processed by CNM (circles), Micron (squares), and ST (triangles). The solid line is the fit of all the experimental data by the function in Eq. (8).

The isothermal annealing of the leakage current density increase rate α is usually fitted by a function, which accounts for an exponential and a logarithmic term, predicting the absence of a saturation value in the long-term characteristics [2]:

$$\alpha(t) = \alpha_0 \exp(-t/\tau_0) + \alpha_1 - \alpha_2 \ln(t/t_2). \quad (7)$$

The leakage current density annealing curve $J_D(t) = \alpha(t)\phi$ can be consequently fitted by the same function of Eq. (7) multiplied by the delivered fluence, and data in Fig. 4 are expected to be fitted by the function

$$\frac{J_D(t)}{J_D(4\,\text{min})} = \frac{\alpha_0 \exp(-t/\tau_0) + \alpha_1 - \alpha_2 \ln(t/t_2)}{\alpha_0 \exp(-4\,\text{min}/\tau_0) + \alpha_1 - \alpha_2 \ln(4\,\text{min}/t_2)}. \quad (8)$$

The α_i values ($i = 0, 1$, and 2) in Eq. (8) can be determined unless a common multiplication factor and have been normalized to α_2. The parameters in Eq. (8) minimizing the least squares from the data of Fig. 4 are $\alpha_0 = 2.12 \pm 0.17$ A/cm, $\alpha_1 = 11.87 \pm 0.70$ A/cm, $\alpha_2 = 1.00 \pm 0.06$ A/cm, $\tau_0 = 9.79 \pm 1.0$ min, if t_2 has been fixed to 1 min according to Ref. [2]. The $J_D(t)/J_D(4\,\text{min})$ experimental data for short annealing times present the expected exponential dependence. The kink of the fitting curves between the 4th (32 min) and 5th (64 min) annealing step indicates that for higher annealing times the exponential becomes negligible and the logarithmic term predominates. In the long-term characteristics the annealing curves well follow the logarithmic time dependence, at least up to 1024 min.

8. Conclusions

Diodes processed by three different manufacturers (CNM, ST Microelectronics and Micron Semiconductor) on standard and oxygenated silicon substrates have been irradiated by nuclear reactor neutrons.

The acceptor introduction rates (β) of standard and oxygenated diodes produced by the same manufacturer are generally compatible, as expected from literature. On the contrary, β significantly varies when standard and oxygenated devices produced by the three different manufacturers are considered, showing that the β dependence on processing can be relevant. In conclusion for the neutron irradiations, the acceptor introduction rate of the oxygenated devices does not appear as a low bond (as found when devices are irradiated with charged hadrons) and processing is the dominant effect.

On the other hand, the leakage current density increase rate (α) is independent of manufacturer process and/or substrate oxygenation. The hardness factor of the irradiation source has been determined to be $K(n_R) = 0.89 \pm 0.01$, which is in agreement with previous measurements.

The N_{eff} reverse annealing amplitude (N_C) is lower for oxygenated than standard devices of the same manufacturer suggesting that a positive effect of the substrate oxygenation exists even for neutron irradiated device. On the other hand, the time parameters of the reverse annealing (τ and t_0) are not significantly affected by processing and/or oxygenation.

The leakage current density as a function of the annealing time ($J_D(t)$) continuously decreases due to the annealing of the radiation induced microscopic defects contributing to the generation current. The $J_D(t)$ data are independent of processing and/or oxygenation and have been successfully fitted by a function which accounts for an exponential and a logarithmic term,

predicting the absence of a saturation value in the long-term characteristics.

References

[1] CMS Collaboration, The Tracker Project: Technical Design Report, CERN/LHCC 98–6, CMS TDR 5, 15 April 1998.
[2] M. Moll, et al., Nucl. Instr. and Meth. A 426 (1999) 87.
[3] S.J. Bates, et al., IEEE Trans. Nucl. Sci. NS43 (1996) 1002.
[4] G. Lindstrom, et al., Nucl. Instr. and Meth. A 426 (1999) 1.
[5] A. Ruzin, et al., Nucl. Instr. and Meth. A 426 (1999) 94.
[6] A. Ruzin, Nucl. Instr. and Meth. A 447 (2000) 116.
[7] G. Casse, et al., IEEE Trans. Nucl. Sci. NS47 (2000) 527.
[8] D. Bisello, et al., Il Nuovo Cimento A 112 (1999) 1377.
[9] J. Wyss, et al., Nucl. Instr. and Meth. A 457 (2001) 595.
[10] D. Bisello, et al., IEEE Trans. Nucl. Sci. NS48 (2001) 1020.
[11] A. Candelori, et al., IEEE Trans. Nucl. Sci. NS48 (2001) 2270.
[12] Z. Li, IEEE Trans. Nucl. Sci. NS42 (1995) 224.
[13] A. Ruzin, et al., Nucl. Phys. B (Proc. Suppl.) 78 (1999) 645.
[14] A. Ruzin, et al., IEEE Trans. Nucl. Sci. NS46 (1999) 1310.
[15] M. Moll, et al., Nucl. Instr. and Meth. A 439 (2000) 282.
[16] B. Dezillie, et al., IEEE Trans. Nucl. Sci. NS47 (2000) 1892.
[17] Z. Li, et al., Nucl. Instr. and Meth. A 461 (2001) 126.
[18] G. Lindstrom, et al., Nucl. Instr. and Meth. A 465 (2001) 60.
[19] G. Lindstrom, et al., Nucl. Instr. and Meth. A 466 (2001) 308.
[20] Institut de Microelectronica de Barcelona (IMB-CNM-CSIC), Barcelona, Spain.
[21] ST Microelectronics, Catania, Italy.
[22] Micron Semiconductor, Lancing, Sussex, UK.
[23] G. Casse, et al., Nucl. Instr. and Meth. A 438 (1999) 429.
[24] L. Fonseca, et al., Microelectron. Reliab. 40 (2000) 791.
[25] V. Cindro, et al., Nucl. Instr. and Meth. A 450 (2001) 288.
[26] A. Chilingarov, et al., Nucl. Instr. and Meth. A 360 (1995) 432.
[27] T. Ohsugi, et al., Nucl. Instr. and Meth. A 265 (1988) 105.
[28] E. Barberis, et al., Nucl. Instr. and Meth. A 326 (1993) 373.
[29] M. Moll, et al., Nucl. Instr. and Meth. B 186 (2002) 110.
[30] D. Žontar, et al., Nucl. Instr. and Meth. A 426 (1999) 51.